

Performance Evaluation on Indoor Positioning System Using SS Ultrasonic Waves for Drone Applications

Tatsuki Okada, Akimasa Suzuki

Graduate school of Software and
Information Science

Iwate Prefectural University
020-0693, Sugo Japan

email g231s004@s.iwate-pu.ac.jp
suzuki_a@iwate-pu.ac.jp

Souichirou Masuda

Faculty of Software and
Information Science

Iwate Prefectural University
020-0693, Sugo Japan

email g031q141@s.iwate-pu.ac.jp

Abstract—This study develops a drone positioning system for use in indoor environments, including dark places, inaccessible areas, and ordinary living environments that do not accommodate conventional methods. Various indoor drone applications have been developed, such as drone communication systems and wall surface inspection, which require remote estimation of drone position. For outdoor applications, a Global Navigation Satellite System (GNSS) is generally used to obtain the drone position. However, as the GNSS radio waves cannot reach indoors or between buildings, camera-based methods, such as Simultaneous Localization and Mapping (SLAM), are applied to estimate the drone's position. The system uses noise-resistant, code-division-multiplexed spread spectrum (SS) ultrasonic waves for three-dimensional positioning. Transmitter and receiver hardware is developed using SS ultrasonic waves and the effect of wind and sound of the positioning system during drone operations on the SS ultrasonic positioning is evaluated. Transmitter and receiver hardware is developed using SS ultrasonic waves and the effect of wind and the sound of the positioning system during drone operations on the SS ultrasonic positioning is evaluated. The accuracy of the positioning system is verified through experiments, and the results indicate that a positioning accuracy within 15 cm is possible despite the effects of downwash generated by the drone's wings, and there was no effect of multipath on the positioning error.

Index Terms—Drone; Indoor Positioning System; SS Ultrasonic Waves; Downwash; IoT Devices.

I. INTRODUCTION

This paper is an extension of the paper initially presented at the VEHICULAR 2020 Ninth International Conference on Advances in Vehicular Systems Technologies and Applications [1]. In this paper, we additionally describe a detailed system configuration to store positioning data in cloud storage using Internet of Things (IoT) technology. We studied the robustness of the system to drone noise when using Gold code with the conventional M-sequence. We also compared the experimental results in an anechoic chamber with those in a reverberant experimental environment to study the effect of the reverberation in the tunnel.

Because they can take off and land vertically in small spaces, drones can be used to perform various activities in unstable places where people and vehicles cannot access. Previous studies have investigated the use of drones for many uses, including autonomous search and rescue operations for victims following a disaster [2], meteorological observations [3], and logistics such as home delivery [4].

When used indoors, drones act as communication robots [5]. However, an appropriate distance is required to allow natural and smooth communication between a human and an autonomous mobile robot. To ensure the appropriate positioning in indoor spaces, the drone's coordinates can be used to develop real-time centimeter-order positioning. A relevant study investigated the use of drones for periodic inspection to detect aging degradation of locations where staff are unable to work, such as high walls of tanks and industrial chimneys [6]. Using drones for this purpose is expected to reduce the high cost of these inspections.

Use of drones indoors is more dangerous than outdoors because the drone can easily crash into obstacles such as humans and walls. Thus, it is essential to determine the position of the drone in relation to other objects. As horizontal and vertical relationships are important in these applications, it is essential to obtain absolute coordinates in space. While a Global Navigation Satellite System (GNSS) is generally used to obtain the absolute coordinates of a drone, the GNSS signal is difficult to detect indoors. Simultaneous Localization and Mapping (SLAM) is often used in non-GNSS environments. However, the flight path of a routine inspection is often in a dark place and the walls do not always follow a uniform pattern, causing large errors in SLAM's self-position estimation.

We therefore propose an indoor positioning system for drones using spread spectrum (SS) ultrasonic waves [7]. This system is expected to obtain three-dimensional (3D) coordinates with an accuracy of 10cm. However, the accuracy may be negatively impacted by noise from the propellers or downwash of a drone. Downwash is the wind created by

the drone's propellers. Therefore, in this study, we conduct an experiment to evaluate the positioning accuracy of drone flights during a periodic inspection.

Section II presents related research. Section III provides an overview of indoor positioning systems using SS ultrasonic waves. Section IV examines the drone's robustness against noise for positioning in a no-multi-path situation through an experiment conducted in an anechoic chamber with no reverberation. Section V evaluates the positioning error when the experiment is conducted in an echoing environment with the same system configuration as in Section IV. Section VI compares the results of Sections IV and V. Section VII provides a summary and future perspectives.

II. RELATED AND PREVIOUS WORKS

There does not almost exist positioning method with drones for indoor multi environments, including dark environments, with accuracy under 10cm. Various sensor systems have been investigated for indoor positioning purposes, including pseudo-lites [8] and BLE beacons [9]. Of these, ultrasonic-wave-based systems using the time of flight (TOF) between the time of transmission and the time of reception systems have the lowest cost and greatest accuracy because of their slow propagation speed and ease of improving resolution. However, because these systems use the time-division multiplexing method with on-off keying, which grows increasingly cumbersome as the number of objects to be measured increases, they generally have weak noise resistance and are slow to acquire data. Systems using SS ultrasonic signals have therefore been investigated to overcome these drawbacks [10] [11].

Analogous to SS radiowave systems (e.g., global positioning system (GPS)), we have proposed a real-time 3D positioning system using SS ultrasonic signals with a band-limited transducer, a low-power field programmable gate array (FPGA), and a small microprocessor [12]. In previous studies, we discussed factors such as positioning errors in indoor environments [7] and showed the measurement accuracy of the positioning system using SS ultrasonic signals. We also proposed a calculation algorithm based on the Newton-Raphson method for continuous signals, rather than conventional pulse signals. As a result, 3D coordinates can be obtained every 80ms using Code Division Multiple Access (CDMA) with continuous signals [13].

We evaluated the positioning accuracy of SS ultrasonic waves using a ground-based mobile robot [14]. Other studies have proposed using not only SS ultrasonic waves but also image sensors for drone positioning [15] and applying drones to limited situations such as greenhouses [16]. Indoor positioning accuracy has been discussed using the Kinect camera, with an average positioning error of 48mm [17]. However, the Kinect is difficult to use in the dark. This study develops an indoor positioning system using only SS ultrasonic waves that can be used in dark places where image sensors are ineffective.

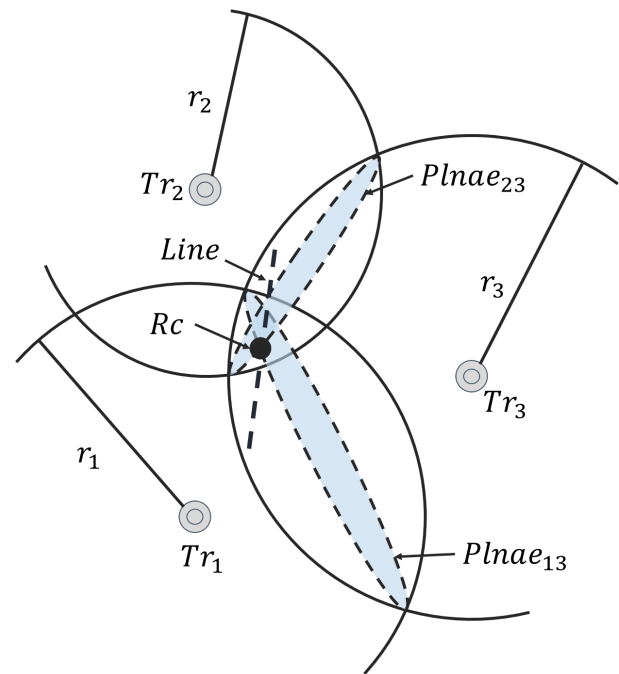


Figure 1. Positioning calculations for the indoor positioning system.

III. INDOOR DRONE POSITIONING SYSTEM USING SS ULTRASONIC SIGNALS

This section describes the indoor positioning method using SS ultrasonic waves and our proposed system.

A. A method for positional calculation

Figure 1 presents the positioning calculations for the indoor positioning system using SS ultrasonic waves. Spheres are drawn to determine the center point on the radius between a receiver R_c and each transmitter. Two pairs of spheres are selected centering on Tr_1 and Tr_3 and Tr_2 and Tr_3 , respectively. From these pairs of spheres, $Plane_{13}$ and $Plane_{23}$ are solved simultaneous equations and a line of intersection is obtained from the two planes. Finally, the points at the intersection of the line with an equation of an arbitrary sphere are solved. Figure 2 shows a flowchart of the algorithm for the positioning calculation in Figure 1. Two intersection points are obtained as two transmitters are installed along the bottom or sides of the positioning range. Therefore, one solution is outside the room and the other solution becomes the position of the receiver R_c . When using four transmitters, four position results are obtained. Thus, the measurement position is defined as an average of these results.

B. Hardware structure of a positioning system using SS ultrasonic waves

A 3D position can be calculated on the basis of three or more TOF between the transmitters and the receiver. Figure 3 shows the system architecture of the TOF measurement for the positioning system. The transmitting hardware contains a digital to analog (D/A) converter and an FPGA to generate carrier

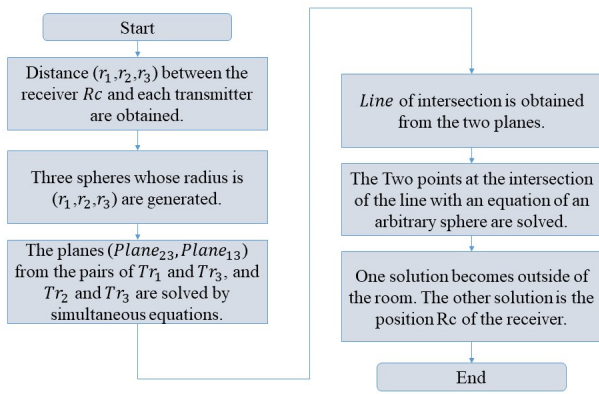


Figure 2. Flowchart of position calculation.

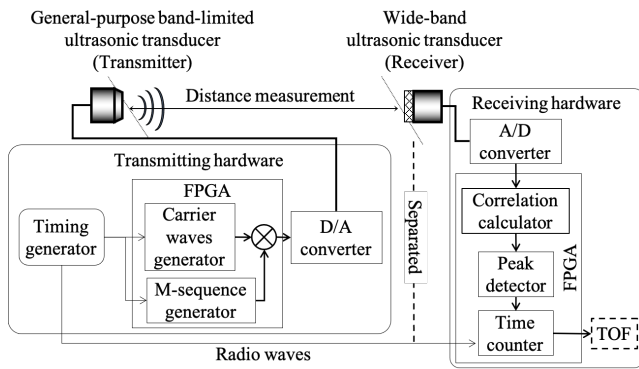


Figure 3. System architecture of the TOF measurement.

waves and M-sequences. The receiving hardware includes an A/D converter and an FPGA for correlation calculation, peak detection, and time measurement.

An SS signal is generated by the transmitting hardware to multiple carrier waves by M-sequences and is output from a transducer after D/A conversion. At the start of the transmission, a time counter is started to measure the TOF and correlation values are calculated from the sound data via the A/D converter as online and real-time hardware processing. The time counter measures the TOF by counting the sampling times until arriving at peak correlation values obtained by the peak detector. Then, the 3D position of the receiver can be calculated based on three or more TOFs between the transmitters and receiver. The correlation calculator component is installed in the hardware as shown in Figure 3. Distance is calculated from the TOF obtained from the hardware and the dimensional position is measured. Real-time positioning is sufficiently available because this processing can be calculated with low cost using optimized expressions.

C. SS signal

In our indoor positioning system, SS signals are modulated by binary phase shift keying using an M-sequence with a direct sequence method. Figure 4 shows the M-sequence generator. ‘0’ or ‘1’ sequence is generated by the shift register.

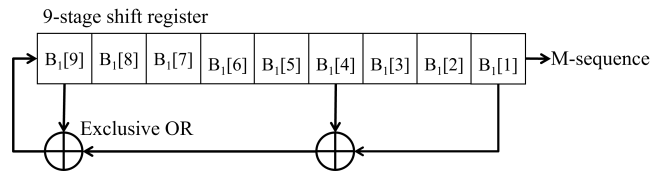


Figure 4. M-sequence generator with tap 4,9.

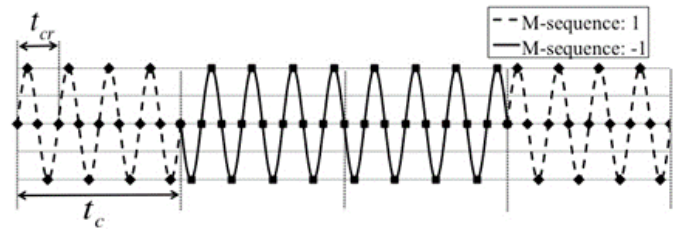


Figure 5. Spread spectrum (SS) ultrasonic signal.

Each number in [] in B_1 of Figure 4 means the number of bits. Tap is defined as a position where exclusive OR calculation is performed. In the case of Figure 4, tap position is shown as {4,9}, which named by the shift register where connected to exclusive OR gates. By changing the position of the tap, several M-sequences with low cross-correlation can be generated.

Figure 5 shows a received SS signal, where the signals corresponding to ‘1’ and ‘-1’ are plotted solid and dashed lines, respectively. We replace values of ‘-1’ with ‘0’ from generated M-sequence for easy signal processing. Each dot in Figure 5 is a sample to convert to digital signals. The amount of sample including one period of carrier waves is decided on the basis of four samples. Here, chip length t_c is defined as the time required to describe a 1-chip of the M-Sequence. The chip length can also be described as $t_c = 4/f$ using carrier frequency f . The length of SS ultrasonic signals becomes $2^9 - 1 = 511$ [chip] owing to a 9-stage shift register for the M-sequence in our system. These four channels of the transmitters are generated by the following tap positions: {4,9}; {3,4,6,9}; {4,5,8,9}; and {1,4,8,9}.

The M-sequence has few combinatorial channels and limited cross-correlation. Therefore, to increase the number of channels, Gold codes obtained by multiplied M-sequences are considered. As shown in Figure 6, the Gold code is generated by using two shift registers, B_1 and B_2 to generate the M-sequence and combining the two registers by an exclusive OR operation. The following tap positions are used to generate the Gold code: combination of {4,9} and {4,5,8,9}, combination of {3,4,6,9} and {4,5,8,9}, combination of {4,5,8,9} and {1,4,8,9} and combination of {1,4,8,9} and {3,4,8,9}. In this system, the frequency of the carrier waves is 40.2kHz.

D. Our proposed indoor positioning system using SS ultrasonic for drones

In this system, we use a transmitter with a closed-type aperture (PC40-18S, Nippon Ceramic Co., Ltd.) and a “Mini”

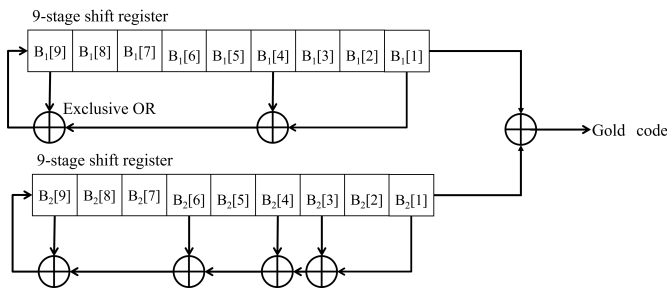


Figure 6. Gold code generated by the M-sequence with tap 9,4 and tap 9,6,4,3.

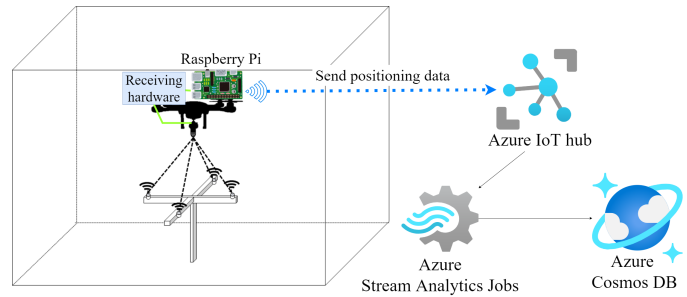


Figure 8. Overview of the sequence to send positioning data from Raspberry Pi to Azure Cosmos DB.

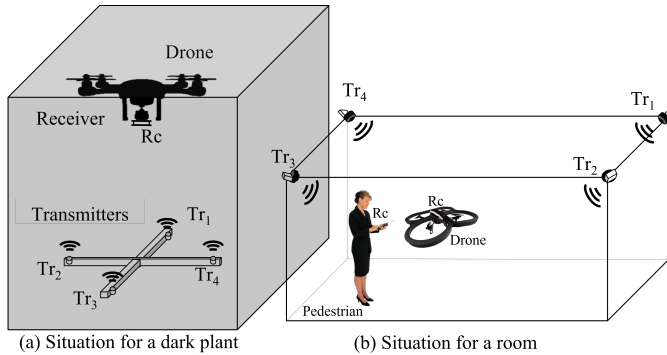


Figure 7. Measurement layout for the proposed system for (a) a dark plant and (b) a room.

Si Sonic™ ultrasonic receiver (SPM0404UD5, Knowles) as general-purpose ultrasonic transducers.

Figure 7 shows the layout of the transmitters and receiver for our proposed system. Two example situations, a dark plant and a room as shown in Figures 7(a) and 7(b), respectively, are used. Figure 7(a) represents a periodical inspection at a plant where it is difficult to install infrastructure, such as transmitters, in the building. For convenient mounting, transmitters are therefore set on a cross-shaped mount, as shown in Figure 7(a). Considering the dilution of precision (DOP) [18] [19], especially horizontal DOP, the larger the mount size, the more accurate the expected positioning accuracy. However, a larger size limits the installation position options and is inconvenient to carry. Figure 7(b) represents a communication drone. Transmitters are mounted in four corners of a room. In this situation, the transmitters are more difficult to install, but the DOP is better than in Figure 7(a). In this study, we conduct experiments using the layout shown in Figure 7(a), because this configuration in Figure 7(a) has not been considered in previous studies.

The sequence to send positioning data to the cloud system is shown in Figure 8. A microphone, receiving hardware, and a Raspberry Pi are mounted on the drone. The positioning data will be sent to Azure CosmosDB using the Microsoft Azure IoT Hub. The data are sent from the receiving hardware to the Azure IoT hub via the Raspberry Pi. In the Azure, the received data are stored in Azure Cosmos DB through Azure Stream Analytics jobs that process and analyze the events in

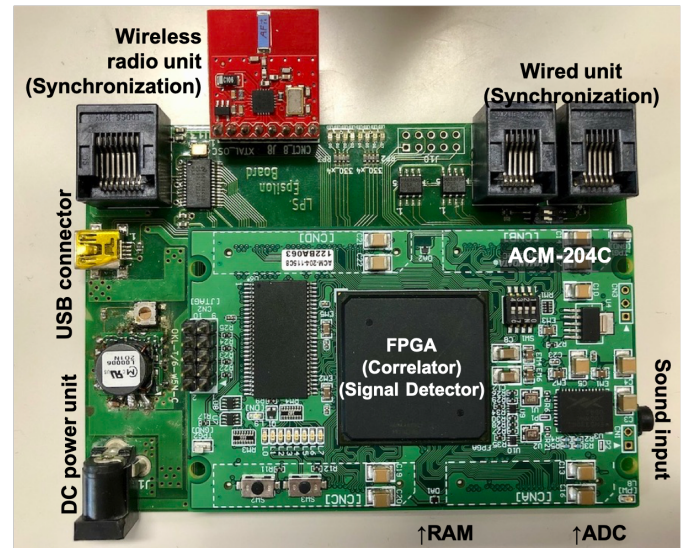


Figure 9. Receiving hardware for drone measurements.

real time. The positioning data can be remotely checked by accessing Azure Cosmos DB online.

Figure 9 illustrates the receiving hardware schematic mounted on the drone, as shown in Figure 8. The hardware consists of an Evaluation Board (ACM204-1158C) installed in the FPGA (Intel Cyclone IV); a transceiver for timing the synchronization of the ultrasonic transmitter unit; a receiver unit; a universal serial bus (USB) interface for output coordinates; an input part to receive the ultrasonic waves, including an A/D converter and amplifier; and synchronous dynamic random-access memory (SDRAM) for the real-time correlation calculations.

The USB interface and the input component are connected to a computer and a microphone, respectively. Ultrasonic waves received by the microphone are converted to A/D and input into the FPGA, where the correlation calculations, peak detection, and TOF calculations are performed. The SDRAM processes the real-time correlation calculations, and the transceiver measures the TOF based on the transmission timing received from the ultrasonic transmitter.

In the Raspberry Pi, the positioning data are calculated by TOF, as obtained by the receiving hardware. Figure 10 shows

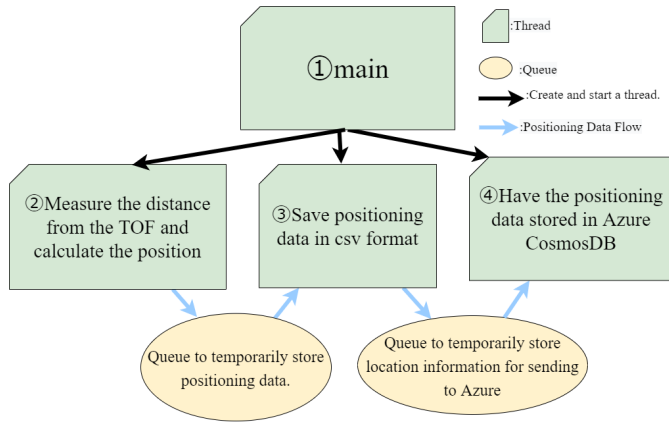


Figure 10. Schematic diagram of the program installed in Raspberry Pi.

an overview of the program running on the Raspberry Pi. This program generates four threads for parallel processing. After the initial setup, we create three threads to run methods, calculates positioning, performs backup, and sending to Azure CosmosDB in parallel. The main thread ① is configured to connect to Azure and USB, and three threads, ②, ③, and ④, are created. In thread ②, the distance d between the receiver and the respective transmitter is measured by the TOF sent from the receiver hardware. The distance is obtained by

$$d = v \times \gamma \quad (1)$$

Here, γ and the v are, respectively, the TOF and the speed of sound calculated by the following approximation formula:

$$v = 331.5 + 0.60714 \times T \quad (2)$$

The temperature $T^\circ\text{C}$ is measured by SENSIRION's SHT31 module [20]. A receiver's position is calculated by four distances from the four transmitters using the method described in Section III-A. At thread ③, the positioning data are saved in CSV format. At thread ④, positioning data are sent to the Azure IoT hub that manages and monitors IoT devices and their communications.

A constant error could occur in the positioning system. More accurate TOF measurement is expected by calibration, which removes this type of error. Thus, in this system, constant errors are removed from measurement results.

IV. POSITIONING EXPERIMENT WITHOUT SOUND REFLECTION.

Before the measurement in a real environment, positioning experiments were conducted in anechoic chamber without sound reflection to study the effect of noise and wind generated by the drone on the distance measurement of SS ultrasonic waves. The experimental environment is shown in Figure 11. The solid line in Figure 11 indicates the environment of the anechoic chamber used, which is 4000mm long, 4100mm wide, and 3000mm high. The area in the dotted line in Figure 11, which is 4000mm long and 2000mm wide, is defined as the comparison area against

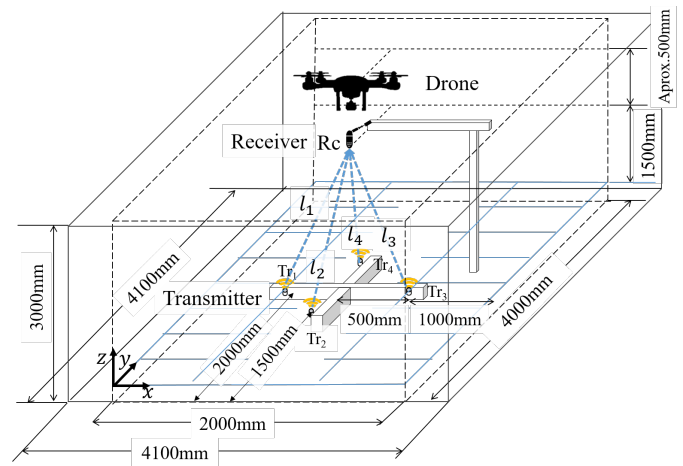


Figure 11. Schematic of the experimental setting in the anechoic chamber.

normal sound reverberation area described in the next section. The lower left corner in this area is defined as the origin of the coordinates. Four transmitters Tr_1 - Tr_4 were placed near the center of the room. The coordinates of the speakers were $Tr_1[\text{mm}] = (500, 2000, 0)$, $Tr_2[\text{mm}] = (1000, 1500, 0)$, $Tr_3[\text{mm}] = (1500, 2000, 0)$, $Tr_4[\text{mm}] = (500, 2000, 0)$, and $Tr_4[\text{mm}] = (1000, 2500, 0)$.

Figure 12 illustrates the anechoic chamber experiment environment. Figure 13 shows the measurement point of the receiver for this experiment. The measurement points to be obtained are Rc_a , which is 1500mm directly above the center of the $x-y$ plane; Rc_b , which is 1500mm directly above Tr_1 ; Rc_c , which is 1500mm directly above Tr_2 ; and Rc_d , which is 1500mm directly above Tr_4 . The transmitter and receiver distances l_1 - l_4 for each measurement point were obtained. The drone was a Mavic 2 zoom by DJI™. The drone hovered approximately 500mm over the receiver. The position was obtained five times at each measurement point. The transmitting waves were $48V_{p-p}$, and both the M-sequence and Gold codes were used in the experiment. For the positioning calculation, the average of the difference of the ultrasonic measured distances was subtracted from the true distance at each point as the constant error from the $l_1 - l_4$ measured distance at each point.

A. RMS positioning error of M-sequence

Figure 14 shows the Root Mean Square (RMS) of the difference between the results and the installed distances. The vertical and horizontal axes of Figure 14 show the RMS positioning error and the coordinates of the measurement points, respectively. em_{rms} is defined as

$$em_{\text{rms}} = \sqrt{(dm_i - d_i)^2} \quad (3)$$

where d_i and dm_i are the measured distance and the true distance between a receiver and i -th transmitter, respectively. The line on the bar in Figure 14 has its upper and lower ends at the maximum and the minimum RMS positioning errors, respectively.

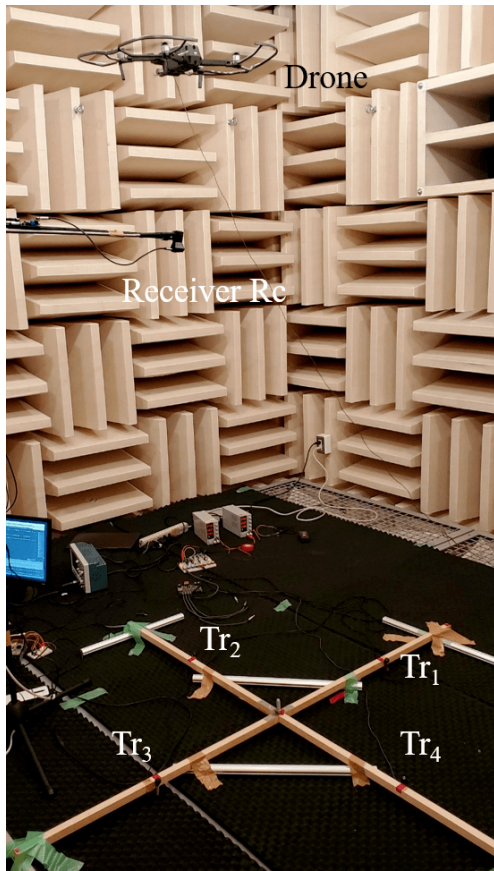


Figure 12. Experimental environment in the anechoic chamber.

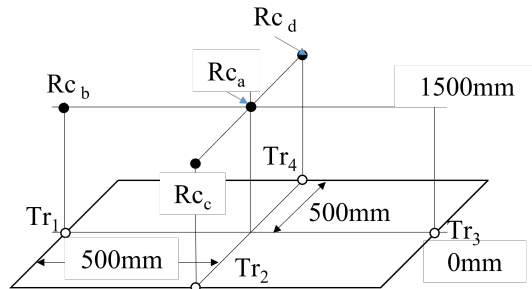


Figure 13. Measurement points of the receivers in Figure 12.

The results show that the range of minimum and maximum RMS positioning errors was wider at all measurement points with the drone because of the sound and wind effects from the drone; however, no other significant trend was identified. The RMS positioning error for all measurement points was within 150mm.

B. Horizontal and vertical errors by M-sequence code

The measurement error on each measurement position was considered for the $x - y$ horizontal error and the z direction error. The horizontal error was calculated as the RMS positioning error of x and y directions on each measurement point. The error in the vertical direction is the absolute value of the

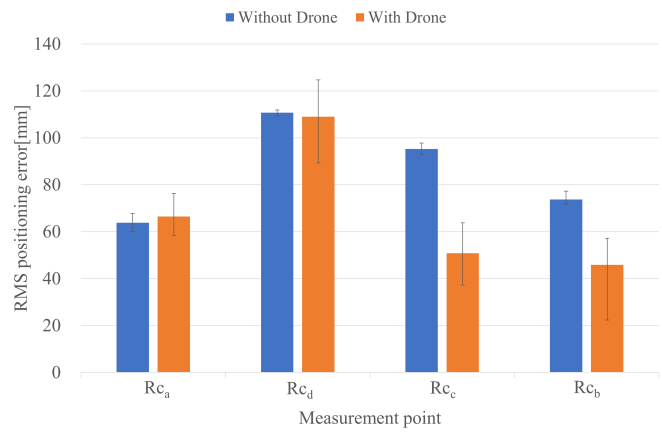


Figure 14. RMS positioning error by M-sequence in an anechoic chamber experiment.

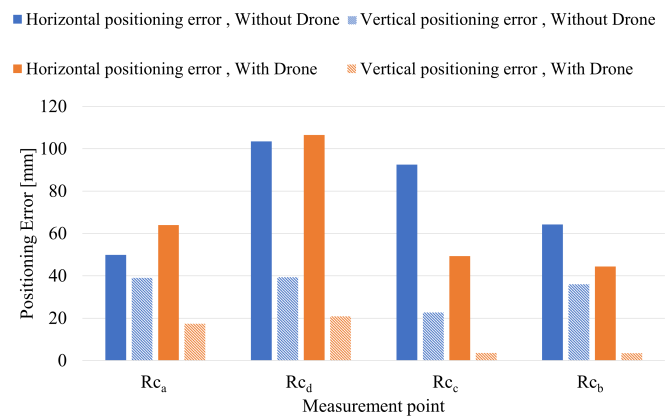


Figure 15. Horizontal and vertical positioning errors by M-sequence code in the anechoic chamber.

error in the z direction. Figure 15 shows the horizontal and vertical errors at each location with and without the drone. The vertical and horizontal axes show the positioning error and measurement point, respectively. Darker and lighter bars in the graph indicate vertical positioning and horizontal positioning errors, respectively.

Figure 15 shows that the horizontal error is larger than the vertical error at all locations. The error in the plane direction is greatly affected by the DOP because the transmitters are placed at a distance of 500mm from the center of the $x - y$ plane. Increasing the interval between the transmitters is expected to improve the accuracy.

C. Comparison of positioning error between Gold code and M-sequence

Figure 16 compares the RMS positioning error after subtracting the constant error of the position using M-sequence and Gold codes. The vertical axis of the graph shows the same RMS positioning error as in Figure 14. The horizontal axis is the measurement point. Similar to Figure 14, the line on the bar in Figure 16 has its upper and lower ends at the maximum

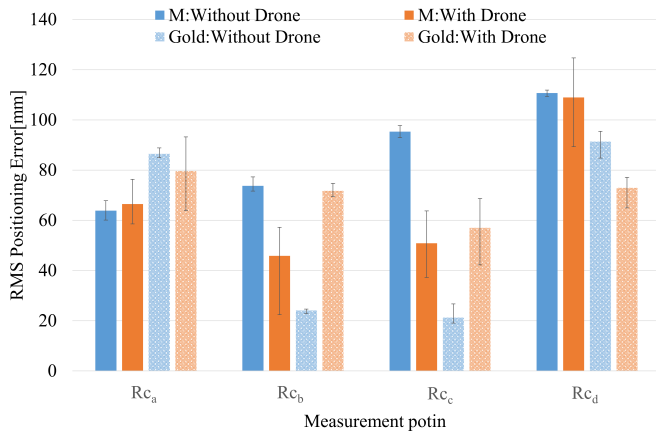


Figure 16. RMS positioning error of Gold code and M-sequence in an anechoic chamber.

and the minimum RMS positioning errors, respectively. The experiment demonstrated that positioning with Gold codes was possible at all points as well as in the M-sequence. Flying the drone increased the range of maximum and minimum RMS positioning errors in the Gold code. In terms of the RMS positioning error between the M-sequence and the Gold code, there was no dominant difference. The RMS positioning errors were 30mm without the drone and 2mm with the drone.

V. POSITIONING ERROR BY DRONE NOISE AND DOWNWASH IN AN INDOOR ENVIRONMENT WITH NORMAL SOUND REFLECTION

In structures such as tunnels, sound reflects off walls, and multi-path effects may occur. To evaluate the effect of motor noise, experiments were conducted in an environment with sound reflection, wind noise, and downwash where reflected waves are generated and comparison is performed with the experiment in the anechoic chamber.

Figure 17 shows the environment used for this experiment, which was a room 2000mm long and 4000mm wide. A Mavic 2 zoom by DJI™ drone as in the anechoic chamber experiment was used. The m-sequence was used as pseudo-random code in this experiment. Four transmitters Tr_1 - Tr_4 were placed near the center of the room. As shown in Figure 17, the drone's starting point was the floor at the left front edge of the room. To prevent the ultrasonic waves from reflecting off the floor, the transmitter was placed at a height of 1500mm above the floor. The coordinates of the transmitters were $Tr_1[\text{mm}] = (500, 2000, 1500)$, $Tr_2[\text{mm}] = (1000, 1500, 1500)$, $Tr_3[\text{mm}] = (1500, 2000, 1500)$, and $Tr_4[\text{mm}] = (1000, 2500, 1500)$. The transmitting SS signal was amplified to $50V_{p-p}$.

Figure 18 shows the experimental environment. SS ultrasonic waves were transmitted upward from Tr_1 - Tr_4 , mounted on a tripod, and received by Rc , mounted on a bridge of wood. Figure 19 shows the measurement point. The white and black circles in Figure 19 denote the transmit and receive points, respectively. Rc_A , $Rc_{A'}$, and $Rc_{A''}$ are the measurement

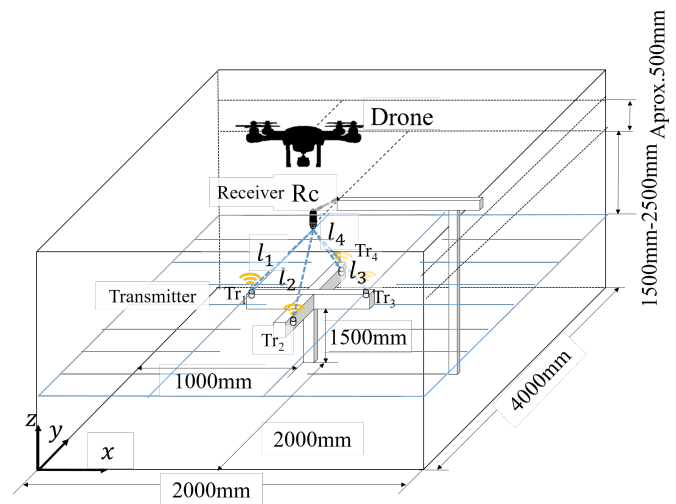


Figure 17. Layout for the positioning experiment in reverberating indoor environment.

points at the center coordinates (1000, 2000, 1500) of the $x-y$ plane of the four transmitters, located 1500mm, 2000mm, and 2500mm above the transmitters, respectively. Rc_C and $Rc_{C''}$ are above transmitter Tr_2 and $Rc_{B''}$ is above transmitter Tr_1 .

The distances, l_1 , l_2 , l_3 , and l_4 , between the transmitters and a receiver (Figure 17) were measured for each measurement point. The drone hovered at a position approximately 500mm above the receiver. The accuracy was examined when the drone was and was not in flight in the environment. Five trials were conducted for each measurement point. As in the Section IV, all experimental results are shown after subtracting the average of the difference from the true value from ultrasonic measured distances.

A. Measurement error in distance in the reverberating Indoor environment

Figure 20 shows the average differences in the distances from the hovering drone for five trials. The vertical and horizontal axes on each graph denote the difference in distance from the drone compared to the measured distance from l_1 to l_4 to Tr_1 to Tr_4 , respectively. The differences in distances are shown as absolute values, and the average difference in the distance is shown as a black line.

The results show that all measured distances could be obtained when the drone was flying, but the measurement distance was affected by the drone's flight. Figure 20(a) shows the drone's distance for the four transmitters, where the measurement point is on the center of the $x-y$ plane. A greater distance between the transmitter and receiver indicates larger measurement distance. Figure 20(b) compares the accuracy of the distance measurement at the center position (1000, 2000) with that when the drone is above Tr_2 at heights of 3000mm and 4000mm. The difference in distance measurement above Tr_2 is the same as that shown in Figure 20(a). The difference in the distance between Tr_2 and $Rc_{C''}$ is increased by the drone hovering. Figure 20(c) shows the measurement distance

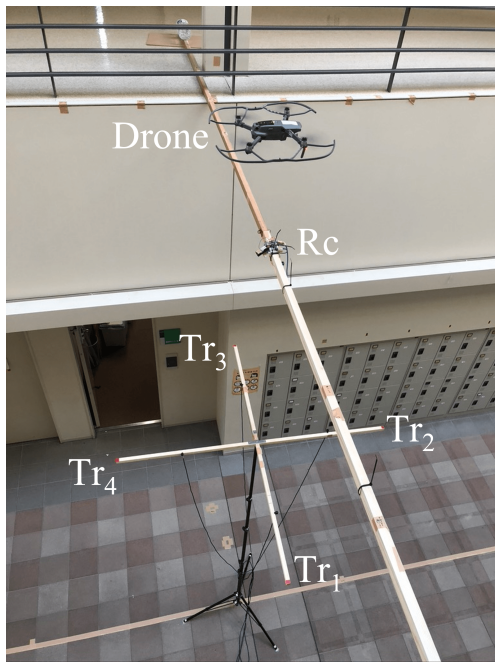


Figure 18. A view of the experiment environment shown from above.

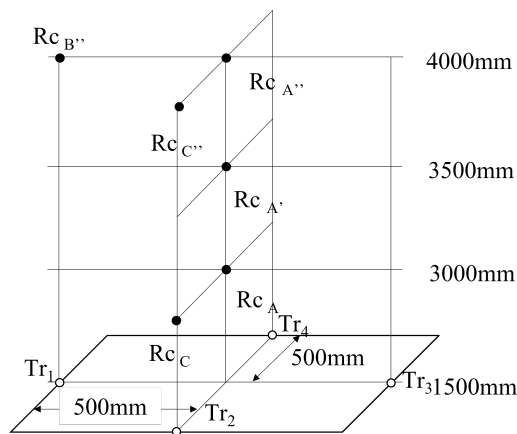


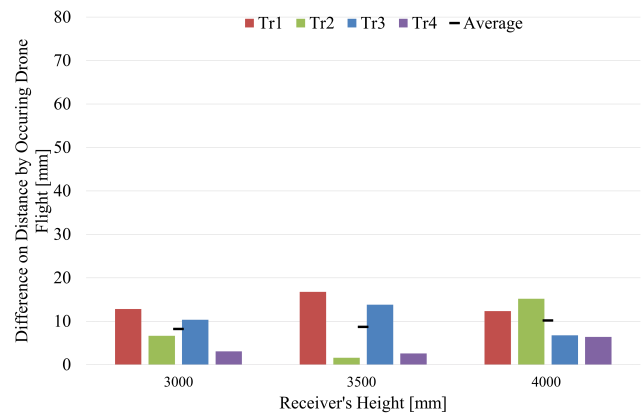
Figure 19. Measurement points of the receivers in Figure 18.

at the height of 4000mm, indicating that the difference in the distance between Tr_1 and $Rc_{B''}$ increases. Compared to $Rc_{A''}$, however, the average difference almost the same.

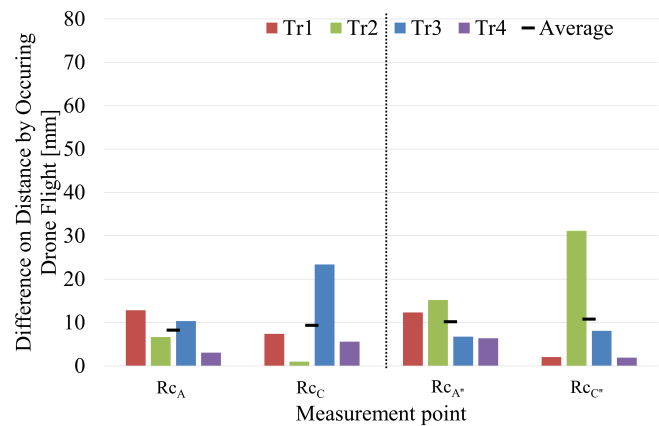
These graphs indicate that a drone's downwash and noise significantly affect the measurement distance when the transmitter and receiver are facing each other. The difference in the measured distance with and without drones is within 4cm.

B. Positioning error in the reverberating indoor environment

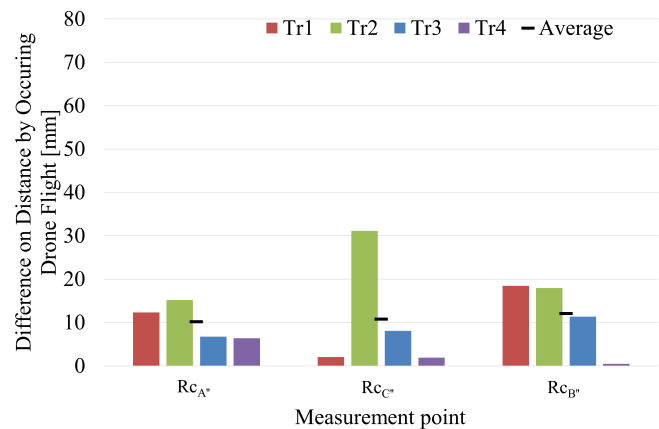
The experimental results were evaluated using the RMS of the difference between the results and the installed distances. Figure 21 shows the RMS positioning errors at the same receivers shown in Figure 20 and the maximum and minimum positioning errors as an expression of variance. The vertical and horizontal axes of Figure 21 denote the RMS positioning



(a) at each receiver's height on the center position



(b) at the center position vs above Tr_2



(c) at a height of 4000mm

Figure 20. Difference in the measured distance due to drone flight for Figure 18 environment.

error and the measurement point, respectively. The positioning errors are an average of five trials.

These results indicate that the positioning error increased when the drone was flying because of downwash and flight noise; however, the average errors were less than 15cm. The

results of Figures 21(a) and (b) confirm that the greater the distance between the transmitter and receiver, the larger the average RMS positioning error and variance when the drone was being flown. Figure 21(c) shows that the most variance was observed at the center of $R_{cA''}$.

These results indicate that the transmission is sufficiently accurate enough to measure a drone for a periodic inner wall inspection. More accurate positioning is expected to be achievable by compensating for errors caused by the angle of the transmitter and receiver and by the measurement distance [21].

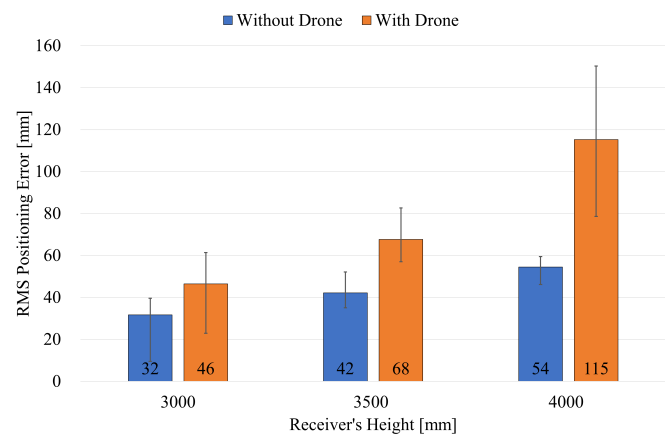
VI. COMPARISON OF RMS POSITIONING ERRORS IN AN ANECHOIC CHAMBER AND A TYPICAL ACCLIMATION ENVIRONMENT

Figure 22 shows the average of all RMS positioning errors acquired in the anechoic chamber and the reverberating indoor environment, respectively, with and without the drone using the M-sequence code. The vertical and horizontal axes in Figure 22, respectively, show the average value of the positioning error for all results and the experimental environment. As with Sections IV and V, the positioning calculation is done after subtracting the average difference from the true value from the ultrasonic measured distances. The line on the bar in Figures 22 and 23 has its upper and lower ends at the maximum and the minimum RMS positioning errors, respectively. As shown in Figure 22, the RMS positioning error in the anechoic chamber and reverberant environment was 32mm with the drone and 10mm without the drone.

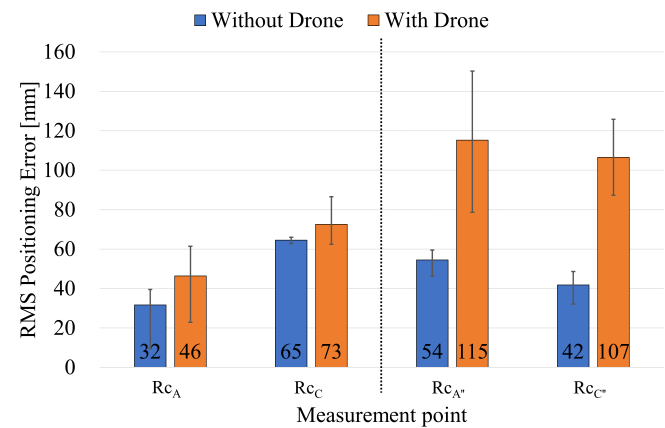
The two positions of R_{c_a} and R_{c_A} as well as R_{c_c} and R_{c_C} have respectively the same transmitter-receiver distance. Figure 23 compares the difference in errors between the anechoic chamber and the reverberating indoor environment. The vertical and horizontal axes show the RMS positioning error and measurement point, respectively. From Figure 23, no trend of the difference in errors could be confirmed. These results show that multi-path has little effect on the positioning results.

VII. CONCLUSIONS AND FUTURE WORK

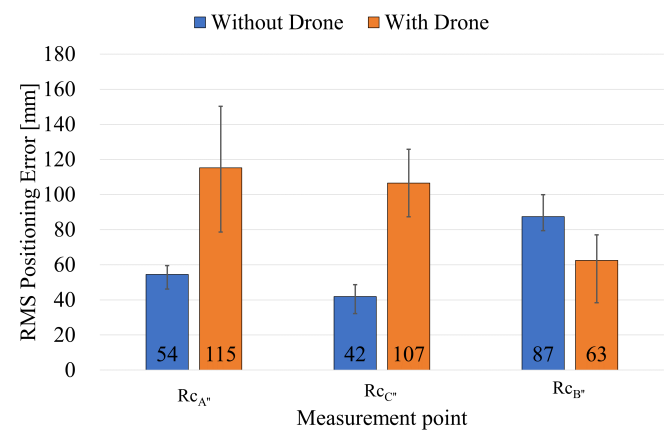
This study proposed a positioning system using SS ultrasonic waves for indoor applications, such as drone communication and wall surface inspection and evaluated the effects of the system against drone downwash and noise. The proposed SS ultrasonic positioning system transmits and receives SS signals using M-sequence, and the distance is measured using the TOF method. From the experiment conducted in an anechoic chamber with no reverberation, the positioning error was within 15cm, although the variance of the error increased due to downwash. The results were compared with the experimental results in a reverberating indoor environment, and the effect of multi-path on the positioning error was not observed. Greater accuracy in the layout of a communication robot is expected because of low DOPs. In terms of DOP, a large error was obtained in the horizontal direction because of the layout of the transmitters in the experimental environment.



(a) at the center position



(b) at the center position vs above Tr_2



(c) at a height of 4000mm

Figure 21. RMS positioning error for Figure 18 environment.

For the positioning of communication robots, higher positioning accuracy is expected owing to the different transmitter layout. Therefore, our positioning system using SS ultrasonic waves can be applied for drone application. We will conduct positioning experiments by SS ultrasonic waves with a drone in an actual tunnel to investigate the usefulness of the proposed

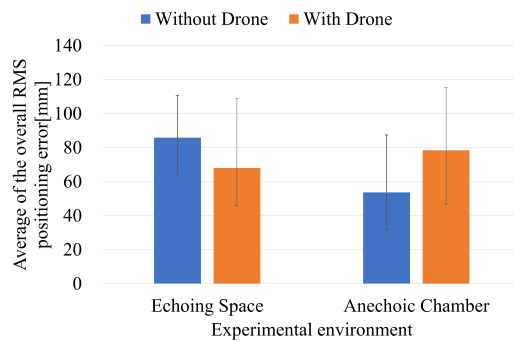


Figure 22. Comparison of average RMS positioning error for all measurement points with anechoic chamber and Figure 18 environment.

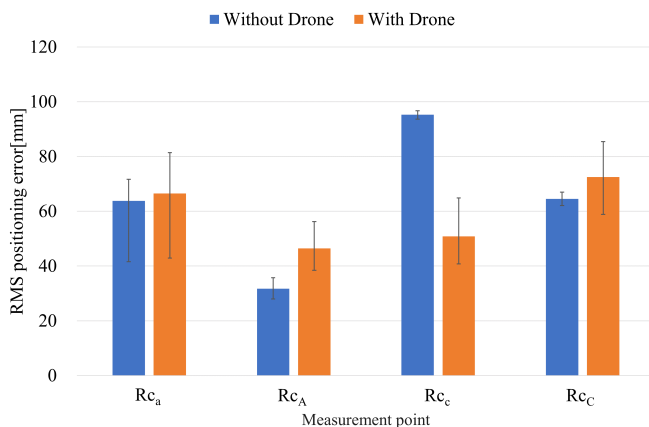


Figure 23. Comparison of RMS positioning error in the same positional relations from the transmitter to receiver with the anechoic chamber and the Figure 18 environment.

system.

ACKNOWLEDGEMENTS

This work was supported by MEXT KAKENHI Grant Number JP 10609423 and Foster Electric Company, Limited. We would like to thank Uni-edit (<https://uni-edit.net/>) for editing and proofreading this manuscript.

REFERENCES

- [1] T. Okada and A. Suzuki, "Measurement accuracy on indoor positioning system using SS ultrasonic waves for drone applications," in VEHICULAR 2020 The Ninth International Conference on Advances in Vehicular Systems, Technologies and Applications, Porto, Portugal, October 2020, pp. 66–71.
- [2] L. Apvrille, T. Tanzi, and J.-L. Dugelay, "Autonomous drones for assisting rescue services within the context of natural disasters," in 31st URSI General Assembly and Scientific Symposium, Beijing, China, Aug 2014, pp. 1–4.
- [3] A. E. MacDonald, "A global profiling system for improved weather and climate prediction," *Bulletin of the American Meteorological Society*, vol. 86, no. 12, Dec. 2005, pp. 1747–1764. [Online]. Available: <https://doi.org/10.1175/bams-86-12-1747>
- [4] W. Yoo, E. Yu, and J. Jung, "Drone delivery: Factors affecting the public's attitude and intention to adopt," *Telematics and Informatics*, vol. 35, no. 6, 2018, pp. 1687 – 1700. [Online]. Available: <http://www.sciencedirect.com/science/article/pii/S0736585318300388>
- [5] U. Nagarajan, G. Kantor, and R. L. Hollis, "Human-robot physical interaction with dynamically stable mobile robots," *Proceedings of the 4th ACM/IEEE international conference on Human robot interaction - HRI '09*, Mar 2009, p. 281–282. [Online]. Available: <http://dx.doi.org/10.1145/1514095.1514176>
- [6] F. Cunha and K. Youcef-Toumi, "Ultra-wideband radar for robust inspection drone in underground coal mines," in 2018 IEEE International Conference on Robotics and Automation (ICRA), Brisbane, Australia, Mar 2018, pp. 86–92.
- [7] A. Suzuki, T. Iyota, Y. Choi, Y. Kubota, K. Watanabe, and A. Yamane, "Measurement accuracy on indoor positioning system using spread spectrum ultrasonic waves," 4th International Conference on Autonomous Robots and Agents, Feb 2009, pp. 294–297.
- [8] X. Gan et al., "Doppler differential positioning technology using the BDS/GPS indoor array pseudolite system," *Sensors*, vol. 19, no. 20. [Online]. Available: <http://dx.doi.org/10.3390/s19204580>
- [9] H. Park, J. Noh, and S. Cho, "Three-dimensional positioning system using bluetooth low-energy beacons," *International Journal of Distributed Sensor Networks*, vol. 12, no. 10, 2016, p. 1550147716671720. [Online]. Available: <https://doi.org/10.1177/1550147716671720>
- [10] M. Hazas and A. Hopper, "Broadband ultrasonic location systems for improved indoor positioning," *IEEE Transactions on Mobile Computing*, vol. 5, no. 5, 2006, pp. 536–547.
- [11] L. Segers, A. Braeken, and A. Touhafi, "Optimizations for FPGA-based ultrasound multiple-access spread spectrum ranging," *Journal of Sensors*, vol. 2020, Jun. 2020, pp. 1–26. [Online]. Available: <https://doi.org/10.1155/2020/4697345>
- [12] A. Suzuki, T. Iyota, and K. Watanabe, "Real-time distance measurement for indoor positioning system using spread spectrum ultrasonic waves," in *Ultrasonic Waves*. InTech, Mar 2012. [Online]. Available: <https://doi.org/10.5772/30215>
- [13] K. Kumakura, A. Suzuki, and T. Iyota, "Code division positioning by continuous signals using spread spectrum ultrasonic waves," *International Conference on Indoor Positioning and Indoor Navigation (IPIN 2013)*, Oct 2013, pp. 1–8.
- [14] A. Suzuki, K. Kumakura, D. Tomizuka, Y. Hagiwara, Y. Kim, and Y. Choi, "Positioning accuracy on robot self-localization by real-time indoor positioning system with SS ultrasonic waves," *Journal of the Korea Society for Power System Engineering*, vol. 17, no. 5, Oct. 2013, pp. 100–111. [Online]. Available: <https://doi.org/10.9726/kspse.2013.17.5.100>
- [15] J. A. Paredes, F. J. Álvarez, T. Aguilera, and J. M. Villadangos, "3D indoor positioning of UAVs with spread spectrum ultrasound and time-of-flight cameras," *Sensors*, vol. 18, no. 2, Dec. 2018, p. 89. [Online]. Available: <https://doi.org/10.3390/s18010089>
- [16] Z. Huang et al., "A noise tolerant spread spectrum sound-based local positioning system for operating a quadcopter in a greenhouse," *Sensors*, vol. 20, no. 7, Apr. 2020, p. 1981. [Online]. Available: <https://doi.org/10.3390/s20071981>
- [17] H. Zhang, G. Chen, Z. Wang, Z. Wang, and L. Sun, "Dense 3D mapping for indoor environment based on feature-point SLAM method," in *Proceedings of the 2020 the 4th International Conference on Innovation in Artificial Intelligence*, ser. ICIAI 2020. New York, NY, USA: Association for Computing Machinery, 2020, p. 42–46. [Online]. Available: <https://doi.org/10.1145/3390557.3394301>
- [18] P. K. Enge, "The global positioning system: Signals, measurements, and performance," *International Journal of Wireless Information Networks*, vol. 1, no. 2, Apr. 1994, pp. 83–105. [Online]. Available: <https://doi.org/10.1007/bf02106512>
- [19] A. Suzuki, T. Iyota, C. Yongwoon, Y. Kubota, K. Watanabe, and A. Yamane, "Measurement accuracy on indoor positioning system using spread spectrum ultrasonic waves," in *ICARA 2009 - Proceedings of the 4th International Conference on Autonomous Robots and Agents*, 03 2009, pp. 294 – 297.
- [20] "Sht3x (rh/t) - digital humidity sensor," 2021, [accessed: 2021-11-29]. [Online]. Available: <https://www.sensirion.com/en/environmental-sensors/humidity-sensors/digital-humidity-sensors-for-various-applications/>
- [21] A. Suzuki and T. Iyota, "Angular dependence of transducers for indoor positioning system using SS ultrasonic waves," *2012 International Conference on Indoor Positioning and Indoor Navigation*, Nov 2012, pp. 1–6.